Human Pilot Interaction with Fast Adapting Flight Control System ⋆

Zoe Mbikayi * **Florian Holzapfel** * **Alexandr Scherbakov** ** **Alexandr V. Efremov** **

* *Institute of Flight System Dynamics, Technical University of Munich, Garching bei München, 85748, Germany (e-mail: zoe.mbikayi@tum.de; florian.holzapfel@tum.de).*
** *Department of Flight Dynamics and Control, Moscow Aviation Institute, Moscow, 125080, Russia (e-mail: pvl@mai.ru).*

Abstract: Interaction between the adaptive behavior of a human pilot and an adaptive flight control system (FCS) usually leads to undesirable adverse effects such as pilot-induced oscillations (PIO). This paper presents an analysis of this interaction in the case of a fast adapting FCS. The analysis shows that, although a pilot will have some nonlinear behavior at the moment when a failure occurs, the fast adapting FCS allows to keep the physical workload low and the pilot behavior remains the same as before the failure. This effectively mitigates the adverse effects seen in the literature.

Keywords: Adaptive control, Data-based control, Fault-tolerant, Modeling of human performance, human-machine interaction

1. INTRODUCTION

Adaptive control is an emerging field, as a means to enhance aviation safety by dealing with unforeseen failures or changes in the dynamics of an aircraft. In the past few years, NASA has tested adaptive control laws on modified F-15 and F/A-18 aircraft, and the results have been mainly successful (Williams (2004); Burken et al. (2006); Page et al. (2006)), with the adaptive controller providing handling qualities ratings (HQR) of 1 to 2 even in case of control surface failure, while the baseline controller provided HQR of 5 to 7. However, these improvements in performance and HQR were not the only result seen in flight tests. Some unexpected interactions between the human pilot and the controlled element were also recorded. One example of this, is the development of roll-axis PIO seen on the flight test results analyzed by Bosworth and Williams-Hayes (2007), during a formation flight with a simulated failed stabilator, while the pitch-axis performance improved. This PIO tendency was experienced by one test pilot while the second test pilot performing the same flight task did not experience any PIO tendency.

These adverse effects have been attributed to the interaction between the adaptive behavior of the human pilot and the adaptive control system, and they are more prominent for larger adaptation times after a failure has occurred (see Trujillo (2014)).

To mitigate these effects, Klyde et al. (2011) suggested to indicate to the pilot that the system being flown has changed, and guide the pilot towards appropriate inputs. This was achieved by introducing a force feedback cues in the active inceptor. The force feedback corresponds to the command path gain adjustment based on the measured error between the adaptive controller response and a nominal system response.

Boskovic et al. (2010) suggested the implementation of a interaction management system works in two main stages. The first stage is the detection of the adverse interactions between the control system and the human, using PIO susceptibility metrics based on the Time-Domain Neal Smith criterion. The second stage is then to generate compensatory input signals that mitigate the adverse effects.

Additionally, from the analysis made by Trujillo (2014), it can be seen that the adverse effects can also be mitigated by simply having an adaptive control system that has fast adaptation times.

This paper presents an analysis of the human pilot behavior in the presence of a fast adapting flight controller, and the influence of the latter on the pilot-vehicle system. The analysis presented is based on human-in-the loop experimental data obtained from ground-based flight tests performed on a supersonic passenger aircraft model, equipped with an adaptive nonlinear dynamic inversion-based controller. The analysis is performed using frequency response and remnant characteristics of the human pilot, which are computed using a Fourier coefficient method.

2. ADAPTIVE CONTROLLER

The control strategy used in this paper consists of a baseline nonlinear dynamic inversion (NDI) control scheme, with an adaptive augmentation that computes the control system coefficients from a system identification module.

⋆ The paper is prepared in the framework of the Program for Development of a World-Class Research Center "Supersonic" in 2020-2025 funded by the Russian Ministry of Science and Higher Education (Agreement dated 16 Nov 2020 No 075-15-2020-924)

2.1 Baseline NDI Control

The nonlinear dynamic inversion control architecture is based on feedback linearization (see Charlet et al. (1989)), through which the aircraft dynamics are canceled using prior knowledge of the said dynamics.

Let the aircraft be described by a set of differential equations as:

$$\dot{x}(t) = f(x) + \gamma(x)u \tag{1}$$
$$y = d(x) \tag{2}$$

where $x(t) \in \mathbb{R}^n$ is the state vector, $u(t) \in \mathbb{R}^m$ is the input vector, and $y(t) \in \mathbb{R}^m$ is the output vector.

If we differentiate the output equation (2) with respect to x, we get equation (3).

$$\dot{y} = \frac{\partial d}{\partial x}\dot{x} = \frac{\partial d}{\partial x}f(x) + \frac{\partial d}{\partial x}\gamma(x)u = F(x) + \Gamma(x)u \tag{3}$$

If the goal is to make the output $\dot{y}$ equal to some pseudo input ν, then the input u that achieves this can be found by inverting equation (3):

$$u = \Gamma^{-1}(x)\left[\nu - F(x)\right] \tag{4}$$

The desired pseudo-input ν can be computed by an error controller such that:

$$\nu = (y_{des} - y)\omega \tag{5}$$

where y_{des} is the desired output, y is the measured output, and ω is the desired bandwidth of the closed loop system.

An integrator can also be added to the error controller in order to improve the robustness of the closed loop system. The schematic realization of this control law can be seen in Fig. 1.

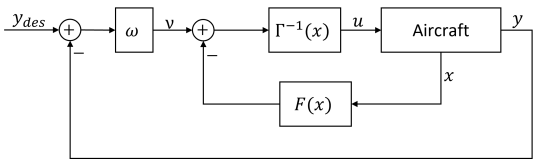

Fig. 1. Nonlinear Dynamic Inversion control scheme

2.2 Adaptive Augmentation

Online System Identification: For online system identification, an algorithm based on mean square minimization is used. The algorithm makes use of a replay buffer that stores a fixed amount of latest flight data points. This means there is a moving window of data used for linear system identification.

Going from the assumption made by Takagi and Sugeno (1985) that a nonlinear system can be approximated by piece-wise linear systems, the linear systems identified using the moving window of data can be used as local linear approximations of the nonlinear system at each time step.

This process goes as follows:

At any operating point, the linear approximation of a nonlinear system can be written as shown in equation (6).

$$\dot{x} = Ax + Bu \tag{6}$$

where $A \in \mathbb{R}^{n\times n}$ is the state matrix, and $B \in \mathbb{R}^{n\times m}$ is the input matrix.

Given a set of l data points of the tuple $[u, x, \dot{x}]$, we can get a system of equations (7), which can be re-written as in equation (8)

$$\begin{cases} \dot{x}_1 = Ax_1 + Bu_1 \\ \dot{x}_2 = Ax_2 + Bu_2 \\ \vdots \\ \dot{x}_l = Ax_l + Bu_l \end{cases} \tag{7}$$

$$Eg = h, \tag{8}$$

where $E \in \mathbb{R}^{l\times(n+m)}$ is a matrix of rank $(n+m)$, with $l \geq (n+m)$ created by concatenation of vectors x and u such that $E = [x, u]$ and g is a matrix containing the solutions A and B such that $g = [A, B]$.

For a linear system, equation (7) holds, which means the A and B matrices are the same for the entire set of data. For a nonlinear system, as the window of data moves, the representative local linear system moves as well. And since this is done at each time step, the result is a near-smooth transition between each local linear system.

This equation can then be solved as shown in equation (9), and the online identification algorithm, making use of the replay buffer can be designed as shown in Fig. 2. The use of a replay buffer allows the algorithm to perform relatively much faster than the usual recursive least squares. The implications of this algorithm are beyond the scope of this paper.

$$g = (E^T E)^{-1} E^T h, \tag{9}$$

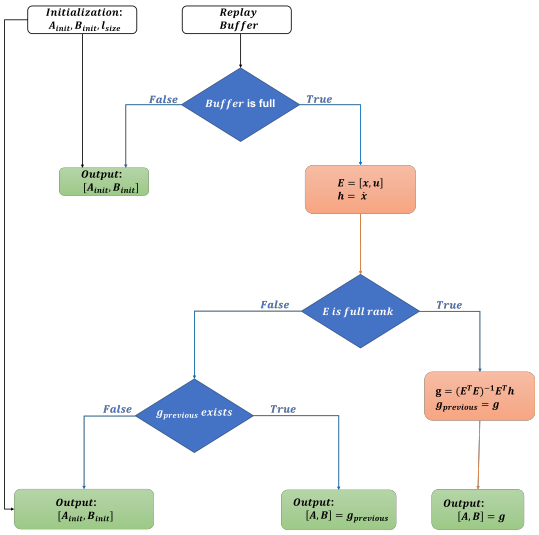

Fig. 2. Online identification algorithm

Control Law: After obtaining the A and B matrices, they can then be used in the control scheme. Assuming the longitudinal dynamics of the aircraft, the differential

equations can be written in state space form as shown in equation (10).

$$\begin{bmatrix} \dot{u} \\ \dot{w} \\ \dot{q} \\ \dot{\theta} \end{bmatrix} = \begin{bmatrix} \chi_u & \chi_w & \chi_q & \chi_\theta \\ Z_u & Z_w & Z_q & Z_\theta \\ m_u & m_w & m_q & m_\theta \\ 0 & 0 & 1 & 0 \end{bmatrix} \begin{bmatrix} u \\ w \\ q \\ \theta \end{bmatrix} + \begin{bmatrix} \chi_\eta \\ Z_\eta \\ m_\eta \\ 0 \end{bmatrix} [\eta] \qquad (10)$$

The pitch rotational equation of motion can be re-written as:

$$\dot{q} = m_u \cdot u + m_w \cdot w + m_q \cdot q + m_\theta \cdot \theta + m_\eta \cdot \eta \qquad (11)$$

Doing the same inversion as in equation (4), we can get the elevator input η that achieves a desired pseudo-input $\nu = \dot{q}$;

$$\eta = \frac{1}{m_\eta}(m_u \cdot u + m_w \cdot w + m_q \cdot q + m_\theta - \dot{q}_d) \qquad (12)$$

The coefficients used in the control law shown in equation (12) are taken from the A and B matrices computed online in the subsection 2.2.

3. EXPERIMENTAL METHOD

3.1 Objective

The objective of the experiments was to analyze the pilot behavior before, during and after a failure has occurred, and the effect of the adaptive controller on the pilot-vehicle system. Two types of failures were analyzed:

(1) Angle of attack feedback failure: Sensor failure is assumed and the angle of attack measurements are therefore unavailable. Given the low static stability of the aircraft used, angle of attack feedback is used in order to provide conventional short period response. Disabling the angle of attack feedback considerably decreases the robustness of any controller in the outer loop.
(2) Elevator failure: The effectiveness of the elevator is sharply decreased by half during the flight.

3.2 Experiment Design

The experiments were designed as a single loop compensatory task (see Fig. 3), and were performed on the MAI ground-based simulator with stereoscopic visual system (see Fig. 4).

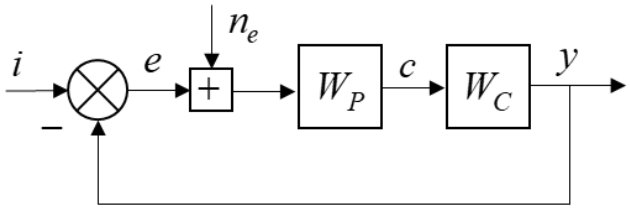

Fig. 3. Pilot-Aircraft system - Compensatory task

where W_P is the human pilot and the W_C is the controlled element dynamics.

The pilot had to complete a compensatory pitch tracking task with a polyharmonic input signal $i(t)$ represented by

Fig. 4. Ground-based simulator

equation (13), which appeared as a random signal to the pilot. The n_e input shown in Fig. 3 represents the remnant of that the pilot introduces in the system.

$$i(t) = \sum_{k=1}^{15} A_k \cos \omega_k t \qquad (13)$$

The amplitudes A_k and orthogonal frequencies $\omega_k = K\frac{2\pi}{T}$ where T is the duration of the experiment, were selected from the requirements of correspondence between the power distributions of the polyharmonic signal and a random signal characterized by the spectral density $\frac{K^2}{(\omega^2+0.5^2)^2}$. The Fourier coefficient technique described by Efremov et al. (1996) was used to calculate the main pilot-vehicle system characteristics.

The starting point is the calculation of the Fourier coefficients $a_k(\lambda)$ and $b_k(\lambda)$ such that:

$$a_k(\lambda) = \frac{2}{T}\int_0^T (\lambda) \cos \omega_k t \quad dt \qquad (14)$$

$$b_k(\lambda) = \frac{2}{T}\int_0^T (\lambda) \sin \omega_k t \quad dt \qquad (15)$$

where (λ) is the signal being analyzed. The Fourier coefficients allow to find the Fourier transform of the of the signal (λ) and the frequency response characteristics at the input frequency ω_k.

The pilot describing function is therefore calculated as:

$$W_p(j\omega) = \frac{C(j\omega)}{E(j\omega)} = \frac{a_k(c) - jb_k(c)}{a_k(e) - jb_k(e)} \qquad (16)$$

where c is the control stick signal, which is the output of the pilot, and e is the error signal, which is the input into the pilot function.

The accuracy of the computed frequency response characteristics depends on some factors, such as the time duration of the signal. Using the modified Fast Fourier Transform (FFT) as shown by Shirley (1969), considerably decreases the time duration needed.

When using FFT, the following requirements need to be fulfilled:

(1) The input frequencies need to be restricted to:

$$\omega_k = \frac{2\pi}{D_k \Delta_t} \qquad (17)$$

where Δ_t is the time interval at which the data is sampled, and D_k should be chosen such that it is divisible by 4.

(2) The ratio $\frac{N}{D_k}$ should be an integer, where N is the number of data samples.

Besides the frequency response characteristics, the pilot remnant the variance of error are computed. As shown by McRuer and Krendel (1974), the pilot remnant represents the nonlinear effects in the behavior of the human pilot. The pilot remnant is an important indicator in the behavior of the pilot especially when a failure occurs, given the fact that the frequency response characteristics are useless in this case. This is because at the moment when a failure occurs, depending on the type of failure, the processes are no longer stationary, and there are nonlinearities both in the dynamics of the aircraft and the adaptive controller.

The error signal E consists of two components: a continuous component, E_i, correlated with the input signal and a discrete component, E_n, correlated with the remnant.

The power of the continuous component E_i is equivalent to the average spectral density given as:

$$P_c(\omega_k) = S_{e_n e_n}(\omega_k)\frac{2\pi}{T} \tag{18}$$

The power of the discrete component E_n, at frequency ω_k, is defined by the amplitude E_k at that frequency such that:

$$P_d(\omega_k) = \frac{E_k^2(\omega_k)}{2} \tag{19}$$

The summarized power of the E signal can then be computed as:

$$\frac{a_k^2(e) + b_k^2(e)}{2} = \frac{E_k^2}{2} + S_{e_n e_n}(\omega_k)\frac{2\pi}{T} \tag{20}$$

By evaluating the Fourier coefficients at two different moment in time T and T', where $T = QT'$, we can get the remnant component E_n:

$$S_{e_n e_n} = \frac{T}{2\pi(Q-1)}\left[\left(\frac{a_k^2(e) + b_k^2(e)}{2}\right)' - \frac{a_k^2(e) + b_k^2(e)}{2}\right] \tag{21}$$

where $P_{T'} = \left(\frac{a_k^2(e)+b_k^2(e)}{2}\right)'$ is the power of the signal of time duration T', and $P_T = \left(\frac{a_k^2(e)+b_k^2(e)}{2}\right)$ is the power of the signal of duration T.

Using $S_{e_n e_n}$, the remnant power spectral density can be computed as:

$$S_{n_e n_e}(\omega_k) = \frac{S_{e_n e_n}}{|W_{CL}(\omega_k)|^2} \tag{22}$$

where $|W_{CL}(\omega_k)|$ is the magnitude of the closed loop system.

The variances can be computed as:

$$\sigma^2(e) = \frac{1}{T}\int_0^T e^2\, dt - \left(\frac{1}{T}\int_0^T e\ dt\right)^2 \tag{23}$$

where $\frac{1}{T}\int_0^T (e)\, dt$ is the mean of the error signal evaluated within the interval T.

Using the Fourier coefficient method , we can get the component of variance correlated with the input signal as:

$$\sigma_i^2(e) = \sum_k \left(\frac{a_k^2(e) + b_k^2(e)}{2}\right) \tag{24}$$

and the remnant part of the variance can then be computed:

$$\sigma_n^2(e) = \sigma^2(e) - \sigma_i^2(e) \tag{25}$$

3.3 Procedure

Several experiments were conducted with the two types of failures introduced. The first series of experiments only used the dynamic inversion controller without the adaptive augmentation and the latter was activated for the second series of experiments.

Each experiment was run for 144 seconds, during which the pilot completed a pitch tracking task. There were three subgroups of experiments:

(1) Before the failure: Experiments are completed with the nominal plant and nominal conditions. The pilot frequency response characteristics and variances of error are recorded.
(2) After the failure: Experiments are completed assuming the failure has already occurred. The dynamics are linear, but the controller is not optimized a-priori to take the failure into account. The pilot frequency response characteristics and variances of error are recorded.
(3) Sudden failure: The experiment starts with nominal conditions, and a failure is introduced after 50 seconds. There are possible nonlinearities at the moment when the failure occurs, and therefore the frequency response characteristics computed cannot be trusted. Therefore only the variances of error with the remnant component of the pilot, and the stick deflection, which is the output of the pilot, can be used to get insight in the behavior of the pilot.

A total number of four pilots performed the experiments, each performing at least 3 experiments for each series. The results shown in the next section are an average of all the experiments performed in each series respectively.

4. RESULTS

4.1 Baseline controller

The experiments were first conducted using only the baseline controller, to be used as a reference point. The pilot frequency response characteristics and variances of error can be seen in Figs. 5 and 6 respectively.

We can see several peaks in the phase characteristics in case of failures representing the significant lead/ lag that the pilot has to introduce to keep the aircraft controllable. We can also see, from the amplitude, that the frequency at which the pilot stops being a constant and starts developing lead has decreased (at roughly 3 rad/s) compared to "before failure" (6 rad/s). Together with the high remnant and seen in 6, this is indication of high pilot workload, low controllability of the aircraft and high PIO probability. Which should be expected, given the nature of the failures.

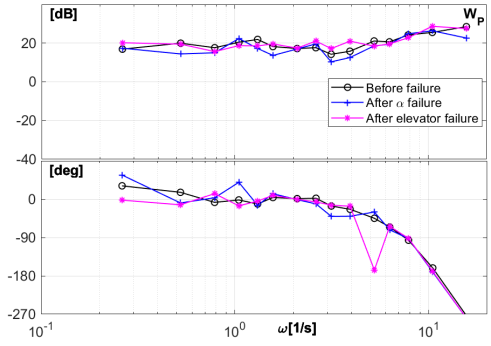

Fig. 5. Pilot frequency response characteristics - Baseline

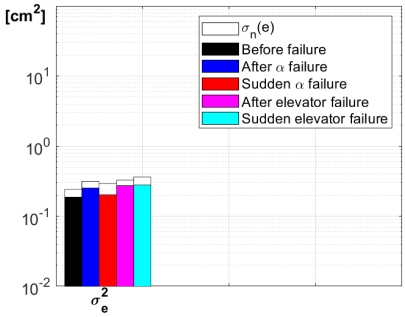

Fig. 6. Variances of error - Baseline

4.2 Adaptive controller

The results of experiments with the adaptive controller are shown in Figs. 7 and 8.

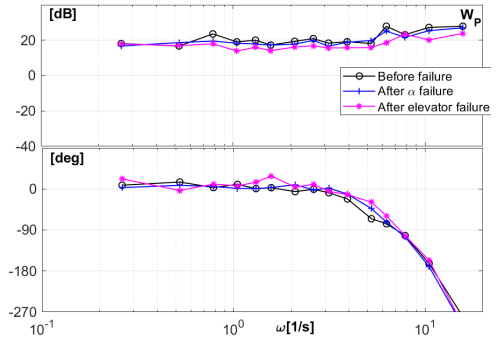

Fig. 7. Pilot frequency response characteristics - Adaptive

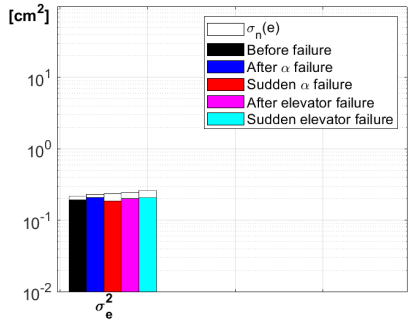

Fig. 8. Variances of error - Adaptive

When the adaptive controller is used, the frequency at which the pilot starts generative lead is kept at 6 rad/s even after the failures, and the phase characteristics are roughly the same, without any concerning peaks as seen previously. This indicates that the pilot workload has not changed, and the pilot interaction with the aircraft is good enough to avoid PIO events.

4.3 Overview

The frequency response characteristics shown previously give no insights into the behavior of the pilot at the moment when the failure occurs. The variances of error correlated with the input signal and correlated with the remnant allow us to get this insight.

The values of the variances seen in the previous subsections are shown in Table 1.

Table 1. Variances of error

	Baseline		**Adaptive**	
	$\sigma^2(e)$	$\sigma_n^2(e)$	$\sigma^2(e)$	$\sigma_n^2(e)$
Before failure	0.2405	0.0540	0.2190	0.0267
After α failure	0.3137	0.0625	0.2305	0.0233
After elevator failure	0.3288	0.0564	0.2455	0.0455
Sudden α failure	0.2926	0.0916	0.2342	0.0477
Sudden elevator failure	0.3603	0.0829	0.2615	0.0615

The first peculiarity that can be noticed when there is only a baseline controller, is that after the failures have occurred, the pilot has difficulties flying the aircraft. This can be seen from the peaks in the phase characteristics, showing that the pilot has to introduce significant phase lead or lag at different frequencies, when compared with the characteristics before the failure.

In the case when there is a sudden failure occurring at 50 seconds, with the baseline controller, the variance of error is up to 39.88 % worse than without failures. And the remnant of the pilot is up to 51.64 % worse. This demonstrates the nonlinearities in the pilot behavior, which, together with the phase lead/ lag that the pilot needs to add, show the high workload of the pilot, high PIO probability and deterioration of the handling qualities. This high workload can also be seen in Fig. 9. After the failure injection, the stick output increased both in amplitude and frequency, and there is visible change of phase.

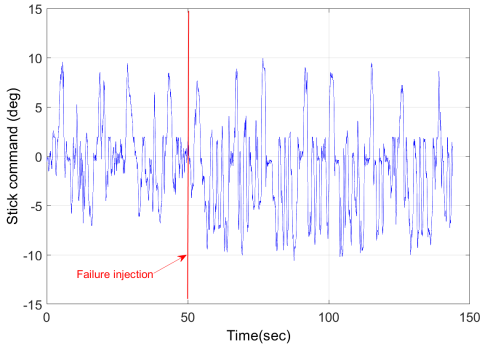

Fig. 9. Pilot output - stick commands (Baseline)

When using the adaptive controller, the adverse effects due to the interaction of the pilot and controller are not present. As said in the introduction of this paper, these effects could be solved by a fast adapting controller. Fig.

10 shows the online adaptation of the entries of the B matrix. There is a low pass filter used to filter out the high frequency noise in the adapted coefficients before using them in the controller.

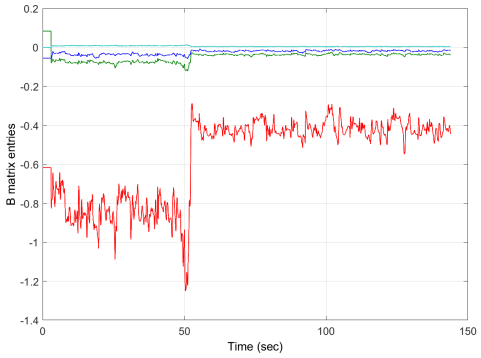

Fig. 10. B-matrix entries - adaptation

As it can be seen, it takes roughly 3 seconds for the adaptation to converge to the new entries in the B matrix after the failure occurs.

Even though this allowed to overcome the adverse effects of the adaptive controller, there is still a significantly higher pilot remnant as seen in Table 1. With a sudden failure, the remnant is 78.9 % worse that the nominal case. This can be explained by the sharp change of the adapted coefficients (see Fig. 10). This coefficients are used directly in the control law. Given the adaptive behavior of the pilot to changes in the controlled element dynamic, this behavior will show nonlinearities when the changes are sudden. However, the pilot workload does not increase, as it can be seen from the stick output (Fig. 11). The characteristics of the pilot output are roughly the same before, and after the failure injection.

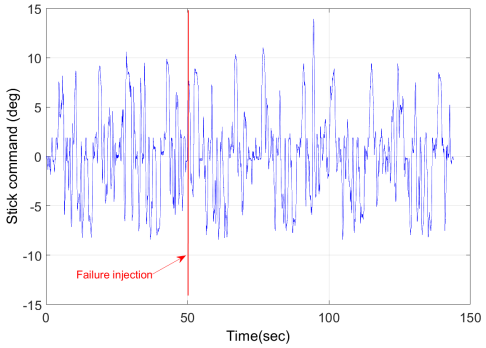

Fig. 11. Pilot output - stick commands (Adaptive)

Additionally, from Fig. 7, it can be seen that after the failure, the frequency characteristics of the pilot are roughly the same as before the failure. The pilot behaves like a constant within the low and mid frequency range. The remnant of the pilot effectively did not change for the case of angle of attack failure, and decreased significantly for the case of elevator failure.

5. CONCLUSION

The results presented above show that using a fast adapting flight control system allows to mitigate the adverse effects that adapting systems have on the pilot-vehicle system. It is seen that the pilot frequency response characteristics remain roughly the same before and after failures. The stick commands, which is the output of the pilot describing function also reveals that the behavior of the pilot remains constant even during the failure. One adverse effect that can be seen is that the fast adapting behavior induces the pilot to also quickly change their gain, which causes a high remnant of the pilot. However, this happens in a very short amount of time and there are no adverse effects on the overall pilot-vehicle system.

REFERENCES

Boskovic, J., Knoebel, N., and Jackson, J. (2010). An initial study of pilot-adaptive controller interactions in flight control. In *AIAA Guidance, Navigation, and Control Conference*, 8016.

Bosworth, J. and Williams-Hayes, P. (2007). Flight test results from the nf-15b intelligent flight control system (ifcs) project with adaptation to a simulated stabilator failure. In *AIAA Infotech Aerospace 2007 Conference and Exhibit*, 2818.

Burken, J.J., Williams-Hayes, P., Kaneshige, J.T., and Stachowiak, S.J. (2006). Adaptive control using neural network augmentation for a modified f-15 aircraft. In *2006 14th Mediterranean Conference on Control and Automation*, 1–6. IEEE.

Charlet, B., Lévine, J., and Marino, R. (1989). On dynamic feedback linearization. *Systems & Control Letters*, 13(2), 143–151. doi:https://doi.org/10.1016/0167-6911(89)90031-5.

Efremov, A.V., Rodchenko, V.V., and Boris, S. (1996). Investigation of pilot induced oscillation tendency and prediction criteria development. Technical report, Wright Lab WL-TR-3109.

Klyde, D., Liang, C.Y., Alvarez, D., Richards, N., Adams, R., and Cogan, B. (2011). Mitigating unfavorable pilot interactions with adaptive controllers in the presence of failures/damage. In *AIAA Atmospheric Flight Mechanics Conference*, 6538.

McRuer, D.T. and Krendel, E.S. (1974). Mathematical models of human pilot behavior. Technical report, ADVISORY GROUP FOR AEROSPACE RESEARCH AND DEVELOPMENT NEUILLY-SUR-SEINE (FRANCE).

Page, A., Monaco, J., and Meloney, D. (2006). Flight testing of a retrofit reconfigurable control law architecture using an f/a-18c. In *AIAA guidance, navigation, and control conference and exhibit*, 6052.

Shirley, R.S. (1969). Application of a modified fast fourier transform to calculate human operator describing functions. *IEEE Transactions on Man-Machine Systems*, 10(4), 140–144. doi:10.1109/TMMS.1969.299913.

Takagi, T. and Sugeno, M. (1985). Fuzzy identification of systems and its applications to modeling and control. *IEEE Transactions on Systems, Man, and Cybernetics*, SMC-15(1), 116–132. doi:10.1109/TSMC.1985.6313399.

Trujillo, Anna C, G.I.M.a.L.E. (2014). Adaptive controller effects on pilot behavior. In *2014 IEEE International Conference on Systems, Man, and Cybernetics (SMC2014)*. IEEE.

Williams, P.S. (2004). Selected flight test results for online learning neural network-based flight control system.